Journal of Petrology, 2024, **65**, egae121. https://doi.org/10.1093/petrology/egae121

Awakening of Maunaloa linked to melt shared from Kīlauea's mantle source

Aaron J. Pietruszka[1], Daniel E. Heaton[2], Jared P. Marske[3], Marc D. Norman[4], Mahinaokalani G. Robbins[1], Reed B. Mershon[1], Kendra J. Lynn[5], Drew T. Downs[5], Arron R. Steiner[6], J. Michael Rhodes[7], Michael O. Garcia[1]

[1]Department of Earth Sciences, University of Hawai'i at Mānoa, Honolulu, HI 96822, USA

[2]Oregon State University, College of Earth, Ocean, and Atmospheric Sciences, Corvallis, OR 97331, USA

[3]Department of Geology, Occidental College, Los Angeles, CA 90041, USA

[4]Research School of Earth Sciences, Australian National University, Canberra ACT 2601, Australia

[5]U.S. Geological Survey, Hawaiian Volcano Observatory, Hilo, HI 96720, USA

[6]School of the Environment, Washington State University, Pullman, Washington 99163, USA

[7]Department of Geosciences, University of Massachusetts, Amherst, MA 01003, USA

*Corresponding author (apietrus@hawaii.edu)

Abstract

Maunaloa—the largest active volcano on Earth—erupted in 2022 after its longest known repose period (~38 years) and two decades of volcanic unrest. This eruptive hiatus at Maunaloa encompasses most of the ~35-year-long Pu'u'ō'ō eruption of neighboring Kīlauea, which ended in 2018 with a collapse of the summit caldera and an unusually voluminous (~1 km^3) rift eruption. A long-term pattern of such anticorrelated eruptive behavior suggests that a magmatic connection exists between these volcanoes within the asthenospheric mantle source and melting region, the lithospheric mantle, and/or the volcanic edifice. The exact nature of this connection is enigmatic. In the past, the distinct compositions of lavas from Kīlauea and Maunaloa were thought to require completely separate magma pathways from the mantle source of each volcano

to the surface. Here, we use a nearly 200-yr record of lava chemistry from both volcanoes to demonstrate that melt from a shared mantle source within the Hawaiian plume may be transported alternately to Kīlauea or Maunaloa on a timescale of decades. This process led to a correlated temporal variation in $^{206}Pb/^{204}Pb$ and $^{87}Sr/^{86}Sr$ at these volcanoes since the early 19th century with each becoming more active when it received melt from the shared source. Ratios of highly over moderately incompatible trace elements (e.g., Nb/Y) at Kīlauea reached a minimum from ~2000 to 2010, which coincides with an increase in seismicity and inflation at the summit of Maunaloa. Thereafter, a reversal in Nb/Y at Kīlauea signals a decline in the degree of mantle partial melting at this volcano and suggests that melt from the shared source is now being diverted from Kīlauea to Maunaloa for the first time since the early to mid-20th century. These observations link a mantle-related shift in melt generation and transport at Kīlauea to the awakening of Maunaloa in 2002 and its eruption in 2022. Monitoring of lava chemistry is a potential tool that may be used to forecast the behavior (e.g., eruption rate and frequency) of these adjacent volcanoes on a timescale of decades. A future increase in eruptive activity at Maunaloa is likely if the temporal increase in Nb/Y continues at Kīlauea.

Key words: Hawai‘i, geochemistry, mantle heterogeneity, melt transport, eruptive behavior

INTRODUCTION

The idea of interaction between Kīlauea and Maunaloa (**Fig. 1a**) is controversial (Klein, 1982; Rhodes et al., 1989; Miklius & Cervelli, 2003; Poland, 2015; Dzurisin & Poland, 2018). Magmatic connections between these volcanoes have been proposed to exist within the asthenospheric mantle source and melting region (Marske et al., 2007), the lithospheric mantle

(Wilding et al., 2023), and/or the volcanic edifice (Rhodes et al., 1989). The shallow (<5 km deep) plumbing systems of Kīlauea and Maunaloa are composed of summit reservoirs that receive mantle-derived magma and deliver it to the rift zones of each volcano (Eaton & Murata, 1960; Poland et al., 2014; Varugu & Amelung, 2021). Their deeper magma transport pathways are poorly resolved, but may converge within the lithospheric mantle at a depth of ~40 km (Wright & Klein, 2006; Wech & Thelen, 2015; Wilding et al., 2023).

Observations from ground deformation (Miklius & Cervelli, 2003; Gonnermann et al., 2012; Poland et al., 2012), seismicity (Burgess & Roman, 2021; Wilding et al., 2023), and eruptive behavior (Klein, 1982) point to a connection between these volcanoes, but the nature of this relationship is enigmatic. An example (**Fig. 1b**) occurred when Maunaloa began inflating from ~2002 to 2008 after a decade of little deformation (Miklius & Cervelli, 2003; Okubo & Wolfe, 2008; Thelen et al., 2017) and Kīlauea experienced a surge in magma supply from ~2003 to 2007 (Poland et al., 2012). This behavior may have been caused by the simultaneous delivery of mantle-derived magma to both volcanoes (Miklius & Cervelli, 2003). Alternately, it may have been an indirect result of rapid melt pressurization within the asthenosphere (Gonnermann et al., 2012) or stress transfer from the plumbing system of one volcano to the other via intrusion of magma within the mantle lithosphere (Burgess & Roman, 2021) or volcanic edifice (Miklius & Cervelli, 2003; Przeor et al., 2022).

A long-standing problem with the idea of a direct magmatic connection between Kīlauea and Maunaloa (i.e., melt mixing) is that the compositional signatures of their lavas (**Fig. 2**) are mostly distinct (see the **Supplementary Materials** for background information on samples, methods, and data sources). This was thought to require completely separate magma pathways from the mantle source region of each volcano to the surface (Wright, 1971; Rhodes et al., 1989;

Frey & Rhodes, 1993; Frey et al., 2016). For example, lavas erupted since the early 19th century at Kīlauea and Maunaloa display no overlap in $^{206}Pb/^{204}Pb$, $^{87}Sr/^{88}Sr$, or ε_{Nd} (**Figs. 2a-b**), which indicates that they are derived from compositionally distinct mantle sources within the Hawaiian plume. These differences extend to ratios of incompatible trace elements (**Figs. 2c-e**) that reflect distinct mantle sources (e.g., Th/Ce and Nb/La) and/or variations in the degree of partial melting (e.g., Nb/Y, Ce/Yb, Zr/Y, and Zr/Nb).

Exceptions are the ~1000-1400 CE lavas from Kīlauea's summit caldera (Kaluapele) at Uēkahuna bluff (**Fig. 1a**) and a few lava flows from Maunaloa dated to ~250-1200 CE (Rhodes et al., 1989; Marske et al., 2007). These lavas converge to an intermediate isotopic composition (defined in **Fig. 2**), hereafter called the "shared" ("S") component of the mantle source because it is observed at both volcanoes. Trace element ratios of these Uēkahuna bluff lavas, and others from two Kīlauea pit craters (Rhodes et al., 1989), partially overlap with the range for Maunaloa. Two models have been proposed to explain this relationship: (1) an invasion of Kīlauea's shallow magmatic plumbing system by magma from Maunaloa following a summit collapse that pre-dated the modern caldera (Rhodes et al., 1989) or (2) the rapid and nearly simultaneous passage of a small-scale compositional heterogeneity through the melting regions of both volcanoes (Marske et al., 2007). In this study, we use a comprehensive dataset of trace element abundances and Pb, Sr, and Nd isotopes ratios to explore the magmatic interaction between Kīlauea and Maunaloa over the last two centuries, and infer the nature of their connection.

RESULTS

The $^{206}Pb/^{204}Pb$ (**Fig. 3a**) and $^{87}Sr/^{86}Sr$ (**Fig. 3b**) ratios of lavas from Kīlauea and Maunaloa display a systematic temporal variation with local extremes from ~1917 to 1921 at Kīlauea and ~1880 to 1907 at Maunaloa. This correlated isotopic fluctuation with a time delay of ~10-40

years is evidence for a magmatic connection between these volcanoes. However, the temporal trends in $^{206}Pb/^{204}Pb$ and $^{87}Sr/^{86}Sr$ cannot be explained by mixing of contemporaneous magmas between the plumbing systems of Kīlauea and Maunaloa, either within the mantle lithosphere (Wilding et al., 2023) or volcanic edifice (Rhodes et al., 1989). Instead, a more complex behavior is observed (inset in **Fig. 2a**). At Maunaloa, lavas from 1843 have among the lowest $^{206}Pb/^{204}Pb$ and highest $^{87}Sr/^{86}Sr$ known for this volcano (Weis et al., 2011), representing an end-member Maunaloa ("M") component in the mantle source. Lavas from 1843 to 1907 trend towards the higher $^{206}Pb/^{204}Pb$ and lower $^{87}Sr/^{86}Sr$ of the shared component (rather than towards Kīlauea lavas erupted since the early 19th century), and thereafter, reverse from 1907 to 1984 towards the Maunaloa end member. Analogous behavior is observed at Kīlauea. Lava from the early 19th century (sample 1820-1) has relatively low $^{206}Pb/^{204}Pb$ and high $^{87}Sr/^{86}Sr$. Lavas from ~1820 to 1921 trend away from the shared component towards the highest $^{206}Pb/^{204}Pb$ and lowest $^{87}Sr/^{86}Sr$ known for this volcano over the last millennium (Marske et al., 2007), representing an end-member Kīlauea ("K") component in the mantle source. Thereafter, Kīlauea lavas from 1929 to 2012 display a reversed trend of decreasing $^{206}Pb/^{204}Pb$ and increasing $^{87}Sr/^{86}Sr$ towards the shared component (rather than towards Maunaloa lavas erupted since the early 19th century).

DISCUSSION

Orthogonal trends between $^{206}Pb/^{204}Pb$ and $^{87}Sr/^{86}Sr$ for Kīlauea and Maunaloa lavas (**Fig. 2a**) require at least three distinct sources within the multi-component Hawaiian plume (Weis et al., 2011, 2020). An isotopically intermediate mantle source is shared by both volcanoes, whereas lavas from each volcano define trends between their respective end-member compositions and this shared component. Similar trends are observed for $^{206}Pb/^{204}Pb$ vs. ε_{Nd} (**Fig. 2b**). This relationship—the lack of direct mixing between the end-member Maunaloa or Kīlauea

components—is inconsistent with the idea (Wilding et al., 2023) that these volcanoes share melt from a common zone of magma storage within the mantle lithosphere. Instead, the magmatic connection between these volcanoes must be related to the generation and transport of melt within the asthenospheric melting region (>80 km deep).

Melt transport from a shared mantle source

The Hawaiian plume is thought to be compositionally heterogeneous on various length scales (**Fig. 4**), ranging from a zonation of tens of kilometers (Frey & Rhodes, 1993; Rhodes & Hart, 1995; Hauri, 1996; Abouchami et al., 2005; Weis et al., 2011; Pietruszka et al., 2013; Frey et al., 2016; Weis et al., 2020) to blobs or filaments <5-10 km in diameter (Marske et al., 2007, 2008; Farnetani & Hofmann, 2010; Greene et al., 2013). Kīlauea and Maunaloa mainly tap compositionally distinct mantle sources, which are inferred to lie separately within the typical melting region of each volcano. A third mantle source—the shared component with intermediate Pb, Sr, and Nd isotope ratios—is likely located between these volcanoes (Marske et al., 2008). The temporal variation in $^{206}Pb/^{204}Pb$ and $^{87}Sr/^{86}Sr$ (**Fig. 3**) can be explained if melt from the shared mantle source is transported alternately to Kīlauea or Maunaloa on a timescale of decades. This suggests that the Hawaiian plume contains a horizontal gradient of compositional heterogeneities (Marske et al., 2008; Pietruszka et al., 2013) rather than a large-scale bilateral asymmetry (Abouchami et al., 2005; Weis et al., 2011; Harpp & Weis, 2020).

Rapid (decades) lateral percolation of melt between the melting regions of Kīlauea and Maunaloa is unlikely (Gonnermann et al., 2012). For example, it would take hundreds of years for melt to travel a horizonal distance of only ~10-20 km by porous flow (Spiegelman & Elliott, 1993) even at the highest rates of mantle upwelling (~10 m/yr) estimated from numerical modeling (Hauri et al., 1994) and ^{230}Th-^{238}U disequilibria (Pietruszka et al., 2001, 2006). Instead,

the melt is likely transferred from interconnected pores into isolated channels within the asthenospheric mantle (Spiegelman & Kenyon, 1992; Hart, 1993; DePaolo, 1996; Katz et al., 2022). These melt transport pathways would efficiently sample small-scale mantle heterogeneities within the Hawaiian plume and rapidly transmit their distinct compositional signatures to the surface (Pietruszka et al., 2006). Melt channels within the asthenosphere might be expected to coalesce upwards into the mantle lithosphere (**Fig. 4**), analogous to the inferred magma transport pathways beneath the Island of Hawai‘i (Burgess & Roman, 2021; Wilding et al., 2023). However, these pathways must remain physically distinct to prevent blending of the end-member Kīlauea and Maunaloa mantle components and preserve the three-component mixing relationships shown in **Figs. 2a-b**.

Mantle controls on eruptive behavior

Further evidence for a magmatic connection between Kīlauea and Maunaloa is based on a broad correlation between changes in lava chemistry—related to the mantle source tapped by each volcano and its inferred degree of partial melting—and their eruptive behavior (**Fig. 3**). For example, modeling of incompatible trace element abundances (Norman & Garcia, 1999; Pietruszka et al., 2013) suggests that the degree of mantle peridotite partial melting is relatively high for Maunaloa (~10%), whereas Kīlauea lavas are produced by a range in melt fractions from ~4% for early 20th century lavas from Kīlauea’s end-member source to ~6% for Pu‘u‘ō‘ō lavas. A higher degree of melting for the shared mantle source (~8%) is predicted by the chemistry of the Maunaloa-like Kīlauea lavas from Uēkahuna bluff (Pietruszka et al., 2013). The lower degree of melting for the end-member Kīlauea source suggests that it is less fertile than either the shared or the end-member Maunaloa sources (Pietruszka & Garcia, 1999; Pietruszka et

al., 2001, 2013). Hereafter, the Nb/Y and Ce/Yb (**Fig. 2c**) ratios of the lavas are used as proxies for the degree of partial melting.

During the early to mid-19th century, Kīlauea (~1820-1832) and Maunaloa (1843) erupted lavas with relatively low $^{206}Pb/^{204}Pb$ (**Fig. 3a**) and high $^{87}Sr/^{87}Sr$ (**Fig. 3b**). Melt from the shared mantle source—melted to a relatively high degree based on the low Ce/Yb of Kīlauea lavas from this period (**Fig. 3c**)—was migrating towards Kīlauea (**Fig. 4a**). A sustained lava lake existed within Kaluapele (and eventually Halema‘uma‘u alone) from at least ~1823 until 1924 (**Fig. 1a**). The early to mid-19th century at Kīlauea was characterized by vigorous caldera-filling eruptions that were punctuated by large (~100 m) summit collapses in 1832, 1840, and 1868. Lava effusion rates at Kīlauea from 1823 to 1840—estimated to be ~0.1 km^3/yr (Pietruszka & Garcia, 1999) or greater (Mastin, 1997)—were relatively high (**Fig. 3d**). No written records exist for Maunaloa eruptions prior to 1843.

By the mid- to late 19th century, melt from the shared mantle source was gradually transferred from Kīlauea to Maunaloa (**Fig. 4b**). The $^{206}Pb/^{204}Pb$ and $^{87}Sr/^{87}Sr$ ratios of Maunaloa lavas from 1843 to 1907 trend towards the shared component. Kīlauea lavas trend away from ~1820 until the early 20th century (~1917 to 1921) when its most isotopically distinct lava erupted (inset in **Fig. 2a**). These trends correlate with changes in Ce/Yb (**Fig. 3c**) that reflect a small increase in the degree of partial melting at Maunaloa (Rhodes & Hart, 1995) and a large decrease at Kīlauea (Pietruszka & Garcia, 1999). During this period, the eruption rate at Kīlauea declined by factor of ~10 (**Fig. 3d**) to a minimum (<0.01 km^3/yr) in the early 20th century (Dvorak & Dzurisin, 1993; Pietruszka & Garcia, 1999), as overflows of Halema‘uma‘u lava lake became less common. In 1924, the lava lake drained, Halema‘uma‘u collapsed, and a series of violent phreatic explosive eruptions (Dvorak, 1992) were followed (after six small summit eruptions) by

the longest known eruptive hiatus at Kīlauea (1934-1952). In contrast, the average rate of lava effusion at Maunaloa was relatively high from 1843 to ~1890 (~0.06 km^3/yr); thereafter, the rate declined to ~0.02 km^3/yr. Thus, the lowest eruption rates at Kīlauea correspond to the highest for Maunaloa (shaded fields on **Fig. 3d**).

Melt from the shared mantle source returned to Kīlauea by the early to mid-20th century (**Fig. 4a**), when there was a change in the trajectory of $^{206}Pb/^{204}Pb$ and $^{87}Sr/^{86}Sr$ for lavas from both volcanoes (inset in **Fig 2a**). Kīlauea lavas trend toward the shared component; Maunaloa lavas trend away. This behavior coincides with a further reduction in the average rate of lava effusion at Maunaloa (**Fig. 3d**) to <0.01 km^3/yr, with only three eruptions after 1950 and its longest known eruptive hiatus (~38 years). The temporal decrease in Ce/Yb at Kīlauea from ~1959 to a local minimum from ~2000 to 2010 indicates that the degree of partial melting increased over this time, consistent with the inferred melting behavior of the shared mantle source. The Ce/Yb trend correlates with an increase in the average eruption rate at Kīlauea—possibly driven by an increase in magma supply (Dvorak & Dzurisin, 1993; Cayol et al., 2000; Poland et al., 2012; Dzurisin & Poland, 2018)—to ~0.04 km^3/yr from the mid-20th century to 1982 and ~0.15 km^3 from 1983 to 2018. Kīlauea erupted frequently from 1952 to 1982. Two major sustained eruptions (**Fig. 1a**) occurred on the volcano's East Rift Zone (ERZ), including Maunaulu (1969 to 1974) and Pu‘u‘ō‘ō (1983 to 2018). The ~2003-2007 surge in magma supply may have led to the formation (in 2008) of the sustained lava lake within Halema‘uma‘u (Poland et al., 2012). This eruptive cycle at Kīlauea culminated in 2018 with the end of the Pu‘u‘ō‘ō eruption and Halema‘uma‘u lava lake, caldera collapse, and a voluminous (~1 km^3) eruption on the ERZ from Ahu‘ailā‘au (Neal et al., 2019).

Recent awakening of Maunaloa

A reversal in the Ce/Yb (**Fig. 3c**) and Nb/Y (**Fig. 1b**) ratios of Kīlauea lavas began after ~2010. This signals a decrease in the degree of mantle partial melting and suggests that melt from the shared mantle source is now being diverted from Kīlauea to Maunaloa for the first time since the early to mid-20th century. Kīlauea erupted five times within Halemaʻumaʻu from 2020 to 2023 at a rate of ~0.09 km^3/yr, which is lower than the long-term average of ~0.15 km^3/yr for Kīlauea from 1983 to 2018 (**Fig. 3d**). The increase in Ce/Yb and Nb/Y at Kīlauea followed a recent change (in ~2002) at the summit region of Maunaloa from deflation to inflation (Miklius & Cervelli, 2003; Thelen et al., 2017; Varugu & Amelung, 2021) and an increase (after ~2004) in seismicity (Okubo & Wolfe, 2008) near Mokuʻāweoweo (**Fig. 1b**). These observations link a mantle-related shift in melt generation and transport at Kīlauea to the awakening of Maunaloa (in ~2002) and first eruption (in 2022) of this "sleeping giant" after nearly four decades of repose.

In summary, Kīlauea and Maunaloa share a source component within the Hawaiian mantle plume in addition to their separate, compositionally distinct end members. Melt from this shared mantle source—most likely located between the two volcanoes (Marske et al., 2008)—may be diverted alternately to Kīlauea or Maunaloa on a timescale of decades (**Fig. 4**). At Kīlauea, lavas from the shared source have lower Ce/Yb (**Fig. 3c**) and Nb/Y (**Fig. 2c**) ratios than lavas from the end-member Kīlauea source due to a relatively large (factor of ~2) difference in the degree of partial melting (Pietruszka et al., 2013). In contrast, all lavas from Maunaloa have low Ce/Yb and Nb/Y ratios because both the shared and end-member Maunaloa sources melt to a relatively high degree. Thus, transfer of mantle-derived melt from Kīlauea to Maunaloa results in an excursion to high Ce/Yb (**Fig. 3c**) and Nb/Y only at Kīlauea.

A histogram (**Fig. 2f**) indicates that low-Nb/Y melt from the shared mantle source was delivered to Kīlauea most of the time over the last millennium. Excursions to high Nb/Y were infrequent. For example, Kīlauea summit lavas from Uēkahuna bluff (~1000-1400 CE) and most of the volcano's rift lavas erupted since the early 19th century have relatively low Nb/Y<0.55. In contrast, nearly all of the lavas with the highest Nb/Y>0.75 (**Fig. 2c**) erupted at Kīlauea's summit from 1912 to 1961 (except for the single analysis of the 1919-1920 Maunaiki rift eruption), which coincides with the early to mid-20th century period of infrequent, small eruptions. This difference suggests that a low magma supply rate at this time made it less likely for the magma with high Nb/Y to reach Kīlauea's rift zones. The only other example of high Nb/Y (~0.8) at Kīlauea (since ~1000 CE) is the heterogeneous MgO-rich glass (up to ~10 wt.%) from the Keanakāko'i Tephra (KT) that erupted in the early to mid-19th century (Garcia et al., 2018; Swanson & Houghton, 2018). All older KT glasses dating back to ~1500 CE have Nb/Y <0.6 (Garcia et al., 2018). The early to mid-19th century KT glasses with high Nb/Y (and high Ce/Yb ~20.2) erupted near the eastern side of the caldera (Swanson & Houghton, 2018), possibly from the deeper of Kīlauea's two summit magma bodies (Poland et al., 2014; Pietruszka et al., 2015) or even bypassing them completely. These glasses likely represent the first delivery of the end-member Kīlauea magma that dominated the chemistry of lavas from the late 19th to early 20th centuries. The rarity of this high-Nb/Y melt indicates that the shared mantle source lies primarily within Kīlauea's typical melting region. The infrequent sharing of this melt with Maunaloa may result from the gradual drift of this volcano away from the center of the Hawaiian plume. This interpretation is consistent with the Kīlauea-like compositions of the oldest studied lavas from Maunaloa (Kurz et al., 1995).

Broader implications

Long-term forecasting of volcanic activity currently relies upon extrapolation of a volcano's past eruptive record to infer its most likely future behavior (Poland & Anderson, 2020). The end-member Maunaloa source and the shared source are both inferred to melt to a higher degree than the end-member Kīlauea source (**Fig. 3d**). Thus, changes in the proportions of the sources tapped by a given volcano—especially at Kīlauea due to the less fertile nature of its end-member source (Pietruszka & Garcia, 1999; Pietruszka et al., 2001, 2013)—may ultimately control the magma supply rate to each volcano. This process would directly affect both the frequency of eruptions and the average rate of effusion, and modulate a broad pattern of anticorrelated eruptive behavior at Kīlauea and Maunaloa (Klein, 1982). Maunaloa will likely erupt more frequently in future decades if the recent increase in Ce/Yb and Nb/Y continues at Kīlauea. Simultaneously, eruptive activity at Kīlauea will likely wane and eventually focus at the volcano's summit, analogous to the century-long eruptive cycle that ended in 1924. We hypothesize that changes in the pathways of melt transport from the heterogeneous Hawaiian plume to the surface (**Fig. 4**)—and the related variations in the magma supply rate—may ultimately be responsible for the cycles of effusive-explosive eruptions at Kīlauea (Swanson et al., 2014) and summit-flank eruptions at Maunaloa (Lockwood, 1995). Monitoring of lava chemistry is a potential tool that may be used to forecast the eruptive behavior of these adjacent volcanoes on a timescale of decades.

Data availability

The data underlying this article are available in the online supplementary material and an EarthChem Library at https://doi.org/10.60520/IEDA/113433.

Acknowledgements

Hawaiian language expert L. Kimura from the University of Hawai‘i at Hilo provided insight into the correct spellings of place names that are used in this paper, including “Maunaloa” as the most prominent example. We thank L. Neymark and M. Vollinger for assistance with the analytical work, L. Hale and the Smithsonian Institution, R. Lee, and D. Swanson for providing samples, and M. Poland and two anonymous reviewers for their thoughtful comments and suggestions. This research was supported by grants from the National Science Foundation (07-38671, 11-18738, and 20-11366 to AJP, and 07-38817, 11-18741, and 14-49744 to MOG). Any use of trade, product, or firm names is for descriptive purposes only and does not imply endorsement by the U.S. Government.

REFERENCES

Abouchami, W., Hofmann, A.W., Galer, S.J.G., Frey, F.A., Eisele, J. & Feigenson, M. (2005). Lead isotopes reveal bilateral asymmetry and vertical continuity in the Hawaiian mantle plume. *Nature* **434**, 851–856.

Burgess, M.K. & Roman, D.C. (2021). Ongoing (2015-) magma surge in the upper mantle beneath the Island of Hawai‘i. *Geophysical Research Letters* **48**, e2020GL091096. https://doi.org/10.1029/2020GL091096.

Cayol, V., Dieterich, J.H., Okamura, A.T. & Miklius, A. (2000). High magma storage rates before the 1983 eruption of Kīlauea, Hawai‘i. *Science* **288**, 2343-2346.

DePaolo, D.J. (1996). High-frequency isotopic variations in the Mauna Kea tholeiitic basalt sequence: melt zone dispersivity and chromatography. *Journal of Geophysical Research* **101**, 11855-11864.

Dvorak, J.J. (1992). Mechanism of explosive eruptions of Kīlauea Volcano, Hawai‘i. *Bulletin of Volcanology* **54**, 638-645.

Dvorak, J.J. & Dzurisin, D. (1993). Variations in magma supply rate at Kīlauea Volcano, Hawai‘i. *Journal of Geophysical Research* **98**, 22255-22268.

Dzurisin, D. & Poland, M.P. (2018). Magma supply to Kīlauea Volcano, Hawai‘i, from inception to now: historical perspective, current state of knowledge, and future challenges. In: Poland, M.P., Garcia, M.O., Camp, V.E. & Grunder, A. (eds), *Field Volcanology: A Tribute to the Distinguished Career of Don Swanson. Geological Society of America Special Paper* **538**, 275-295. https://doi.org/10.1130/2018.2538(12).

Eaton, J.P. & Murata, K.J. (1960). How volcanoes grow. *Science* **132**, 925-938.

Farnetani, C.G. & Hofmann, A.W. (2010). Dynamic and internal structure of the Hawaiian plume. *Earth and Planetary Science Letters* **295**, 231-240. https://doi.org/10.1016/j.epsl.2010.04.005.

Frey, F.A. & Rhodes, J.M. (1993). Intershield geochemical differences among Hawaiian volcanoes: implications for source compositions, melting process and magma ascent paths, *Philosophical Transactions of the Royal Society of London* **342**, 121-136.

Frey, F.A., Huang, S., Xu, G. & Jochum, K.P. (2016). The geochemical components that distinguish Loa- and Kea-trend Hawaiian shield lavas. *Geochimica et Cosmochimica Acta* **185**, 160-181. https://doi.org/10.1016/j.gca.2016.04.010.

Garcia, M.O., Mucek, A.E., Lynn, K.J., Swanson D.A. & Norman, M.D. (2018). Geochemical evolution of Keanakāko‘i Tephra, Kīlauea Volcano, Hawai‘i. In: Poland, M.P., Garcia, M.O., Camp, V.E. & Grunder, A. (eds), *Field Volcanology: A Tribute to the Distinguished Career of Don Swanson* (eds), *Geological Society of America Special Paper* **538**, pp. 203-225. https://doi.org/10.1130/2018.2538(09).

Gonnermann, H.M., Foster, J.H., Poland, M., Wolfe, C.J., Brooks, B.A., Miklius, A. (2012). Coupling at Mauna Loa and Kīlauea by stress transfer in an asthenospheric melt layer. *Nature Geoscience* **5**, 826-829.

Greene, A.R., Garcia, M.O., Pietruszka, A.J., Weis, D., Marske, J.P., Vollinger, M.J. & Eiler, J. (2013). Temporal geochemical variations in lavas from Kīlauea’s Pu‘u ‘Ō‘ō eruption (1983-2010): cyclic variations from melting of source heterogeneities. *Geochemistry, Geophysics, Geosystems* **14**, 4849-4873. https://doi.org/10.1002/ggge.20285.

Harpp, K.S. & Weis, D. (2020). Insights into the origins and compositions of mantle plumes: a comparison of Galápagos and Hawai‘i. *Geochemistry, Geophysics, Geosystems* **21**, e2019GC008887. https://doi.org/10.1029/2019GC008887.

Hart, S.R. (1993). Equilibration during mantle melting: a fractal tree model. *Proceeding of the National Academy of Sciences* **90**, 11914-11918.

Hauri, E.H. (1996). Major-element variability in the Hawaiian mantle plume. *Nature* **382**, 415-419.

Hauri, E.H., Whitehead, J.A. & Hart, S.R. (1994). Fluid dynamics and geochemical aspects of entrainment in mantle plumes, *Journal of Geophysical Research* **99**, 24275-24300.

Katz, R.F., Ree Jones, D.W., Rudge, J.F. & Keller, T. (2022). Physics of melt extraction from the mantle: speed and style. Annual Review of Earth and Planetary Sciences 50, 507-40. https://doi.org/10.1146/annurev-earth-032320-083704.

Klein, F.W. (1982). Patterns of historical eruptions at Hawaiian volcanoes. *Journal of Volcanology and Geothermal Research* **12**, 1-35.

Kurz, M.D., Kenna, T.C., Kammer, D.P., Rhodes, J.M. & Garcia, M.O. (1995). Isotopic evolution of Mauna Loa Volcano: A view from the submarine southwest rift zone. In: Rhodes, J.M. & Lockwood, J.P. (eds), *Mauna Loa Revealed: Structure, Composition, History, and Hazards. American Geophysical Union, Geophysical Monograph* **92**, pp. 289-306.

Lockwood, J.P. (1995). Mauna Loa eruptive history—the preliminary radiocarbon record. In: Rhodes, J.M. & Lockwood, J.P. (eds), *Mauna Loa Revealed: Structure, Composition, History, and Hazards. American Geophysical Union, Geophysical Monograph* **92**, pp. 81-94.

Marske, J.P., Pietruszka, A.J., Weis, D., Garcia, M.O. & Rhodes, J.M. (2007). Rapid passage of a small-scale heterogeneity through the melting regions of Kīlauea and Mauna Loa Volcanoes. *Earth and Planetary Science Letters* **259**, 34-50.

Marske, J.P., Garcia, M.O., Pietruszka, A.J., Rhodes, J.M. & Norman, M.D. (2008). Geochemical variations during Kīlauea's Pu'u 'Ō'ō eruption reveal a fine-scale mixture of mantle heterogeneities within the Hawaiian plume. *Journal of Petrology* **49**, 1297-1318.

Mastin, L.G. (1997). Evidence for water influx from a caldera lake during the explosive hydromagmatic eruption of 1790, Kīlauea Volcano, Hawai'i. *Journal of Geophysical Research* **102**, 20093-20109.

Miklius, A. & Cervelli, P. (2003). Interaction between Kīlauea and Mauna Loa. *Nature* **421**, 229.

Neal C.A., Brantley S.R., Antolik L., Babb J.L., Burgess M., Calles K., Cappos M., Chang J.C., Conway S., Desmither L., Dotray P., Elias T., Fukunaga P., Fuke S., Johanson I.A., Kamibayashi K., Kauahikaua J., Lee R.L., Pekalib S., Miklius A., Million W., Moniz C.J., Nadeau P.A., Okubo P., Parcheta C., Patrick M.P., Shiro B., Swanson D.A., Tollett W., Trusdell F., Younger E.F., Zoeller M.H., Montgomery-Brown E.K., Anderson K.R., Poland M.P., Ball J.L., Bard J., Coombs M., Dietterich H.R., Kern C., Thelen W.A., Cervelli P.F., Orr T., Houghton B.F., Gansecki C., Hazlett R., Lundgren P., Diefenbach A.K., Lerner A. H., Waite G., Kelly P., Clor L., Werner C., Mulliken K., Fisher G. and Damby D. (2019). The 2018 rift eruption and summit collapse of Kīlauea Volcano. *Science* **363**, 367-374, https://doi.org/10.1126/science.aav7046.

Norman, M.D. & Garcia, M.O. (1999). Primitive magmas and source characteristics of the Hawaiian plume: petrology and geochemistry of shield picrites. *Earth and Planetary Science Letters* **168**, 27-44.

Okubo, P.G. & Wolfe, C.J. (2008). Swarms of similar long-period earthquakes in the mantle beneath Mauna Loa Volcano. *Journal of Volcanology and Geothermal Research* **178**, 787-794.

Pietruszka, A.J. & Garcia, M.O. (1999). A rapid fluctuation in the mantle source and melting history of Kīlauea Volcano inferred from the geochemistry of its historical summit lavas (1790-1982). *Journal of Petrology* **40**, 1321-1342.

Pietruszka A.J., Rubin, K.H. & Garcia, M.O. (2001). ^{226}Ra-^{230}Th-^{238}U disequilibria of historical Kīlauea lavas (1790-1982) and the dynamics of mantle melting within the Hawaiian plume. *Earth and Planetary Science Letters* **186**, 15-31.

Pietruszka, A.J., Hauri, E.H., Carlson, R.W. & Garcia, M.O. (2006). Remelting of recently depleted mantle within the Hawaiian plume inferred from the ^{226}Ra-^{230}Th-^{238}U disequilibria of Pu‘u ‘Ō‘ō eruption lavas. *Earth and Planetary Science Letters* **244**, 155–169.

Pietruszka A.J., Norman M.D., Garcia M.O., Marske J.P. & Burns D.H. (2013). Chemical heterogeneity in the Hawaiian mantle plume from the alteration and dehydration of recycled oceanic crust. *Earth and Planetary Science Letters* **361**, 298-309. https://doi.org/10.1016/j.epsl.2012.10.030.

Pietruszka, A.J., Heaton, D.E., Marske, J.P. & Garcia, M.O. (2015). Two magma bodies beneath the summit of Kīlauea Volcano unveiled by isotopically distinct melt deliveries from the mantle. *Earth and Planetary Science Letters* **413**, 90-100. https://doi.org/10.1016/j.epsl.2014.12.040.

Poland, M.P., Miklius, A., Sutton, A.J. & Thornber, C.R. (2012). A mantle-driven surge in magma supply to Kīlauea Volcano during 2003-2007. *Nature Geoscience* **5**, 295-300.

Poland, M.P., Miklius, A. & Montgomery-Brown, E.K. (2014). Magma supply, storage, and transport at shield-stage Hawaiian volcanoes. In: Poland, M.P., Takahashi, T.J. & Landowski, C.M. (eds), *Characteristics of Hawaiian Volcanoes. U.S. Geological Survey Professional Paper* **1801**, pp. 179-234.

Poland, M. P. (2015). "Points requiring elucidation" about Hawaiian volcanoes. In: Carey, R.J., Cayol, V., Poland, M.P. & Weis, D. (eds), *Hawaiian Volcanoes: From Source to Surface. American Geophysical Union, Geophysical Monograph* **208**, pp. 533-562.

Poland, M.P. & Anderson, K.R. (2020). Partly cloudy with a chance of lava flows: forecasting volcanic eruptions in the twenty-first century. *Journal of Geophysical Research* **125**, e2018JB016974. https://doi.org/10.1029/2018JB016974.

Przeor, M., D'Auria, L., Pepe, S., Tizzani, P. & Cabrera-Pérez, I. (2022). Elastic interaction between Mauna Loa and Kīlauea evidenced by independent component analysis. *Science Reports* **12**, 19863.

Rhodes, J.M. & Hart, S.R. (1995). Episodic trace element and isotopic variations in historical Mauna Loa lavas: implications for magma and plume dynamics. In: Rhodes, J.M. & Lockwood, J.P. (eds), *Mauna Loa Revealed: Structure, Composition, History, and Hazards. American Geophysical Union, Geophysical Monograph* **92**, pp. 263-288.

Rhodes, J.M., Wenz, K.P., Neal, C.A., Sparks, J.W. & Lockwood, J.P. (1989). Geochemical evidence for invasion of Kīlauea's plumbing system by Mauna Loa magma. *Nature* **337**, 257-260.

Spiegelman, M. & Elliott, T. (1993). Consequences of melt transport for uranium series disequilibrium in young lavas, *Earth and Planetary Science Letters* **118**, 1-20.

Spiegelman, M. & Kenyon, P. (1992). The requirements for chemical disequilibrium during magma migration. *Earth and Planetary Science Letters* **109**, 611-620.

Swanson D.A. & Houghton, B.F. (2018). Products, processes, and implications of Keanakāko‘i volcanism, Kīlauea Volcano, Hawai‘i. In: Poland, M.P., Garcia, M.O., Camp, V.E. & Grunder, A. (eds), *Field Volcanology: A Tribute to the Distinguished Career of Don Swanson* (eds), *Geological Society of America Special Paper* **538**, pp. 159-190. https://doi.org/10.1130/2018.2538(07).

Swanson, D.A., Rose, T.R., Mucek, A.E., Garcia, M.O., Fiske, R.S. & Mastin, L.G. (2014). Cycles of explosive and effusive eruptions at Kīlauea Volcano, Hawai‘i. *Geology* **42**, 631-634.

Thelen, W.A., Miklius, A. & Neal, C. (2017). Volcanic unrest at Mauna Loa, Earth’s largest active volcano. *Eos*, **98**. https://doi.org/10.1029/2017EO083937.

Varugu, B. & Amalung, F. (2021). Southward growth of Mauna Loa’s dike-like magma body driven by topographic stress. *Scientific Reports* **11**, 9816.

Wech, A.G. & Thelen, W.A. (2015). Linking magma transport structures at Kīlauea Volcano. *Geophysical Research Letters* **42**, 7090–7097. https://doi.org/10.1002/2015GL064869.

Weis, D., Garcia, M.O., Rhodes, J.M., Jellinek, M. & Scoates, J.S. (2011). Role of the deep mantle in generating the compositional asymmetry of the Hawaiian mantle plume. *Nature Geoscience* **4**, 831-838.

Weis, D., Harrison, L.N., McMillan, R. & Williamson, N.M.B. (2020). Fine-scale structure of Earth’s deep mantle resolved through statistical analysis of Hawaiian basalt geochemistry. *Geochemistry, Geophysics, Geosystems* **21**, e2020GC009292. https://doi.org/10.1029/2020GC009292.

Wilding, J.D., Zhu, W., Ross, Z.E. & Jackson, J.M. (2023). The magmatic web beneath Hawai‘i. *Science* **379**, 462-468.

Wright, T.L. (1971). Chemistry of Kīlauea and Mauna Loa lava in space and time. *U.S. Geological Survey Professional Paper* **735**, pp. 1-40.

Wright, T.L. & Klein, F.W. (2006). Deep magma transport at Kīlauea Volcano, Hawai‘i. *Lithos* **87**, 50-79.

Figure captions

Fig. 1. Locations of Kīlauea and Maunaloa, and the relationship between volcanic unrest at Maunaloa and changes in lava chemistry at Kīlauea since 1982. **a**, Map of the Hawaiian Islands (inset) and the southeastern portion of the Island of Hawai‘i, showing the calderas of Kīlauea (Kaluapele) and Maunaloa (Moku‘āweoweo). The approximate location of the Hawaiian mantle plume is indicated by the green oval. Rift zones (orange) extend from Moku‘āweoweo and Kaluapele to the east (ERZ), northeast (NERZ), or southwest (SWRZ). Halema‘uma‘u is a crater within Kaluapele. Uēkahuna bluff lavas are exposed on the northwestern wall of Kaluapele (blue circle). The location of the Pāhala earthquake swarm (Wilding et al., 2023) is indicated by the gray oval. Vent locations for major Kīlauea ERZ eruptions since the mid-20th century are shown by triangles: Maunaulu (1969-1974), Pu‘u‘ō‘ō (1983-2018), and Ahu‘ailā‘au (2018). MOKP and MLSP are two stations used for monitoring of ground deformation at Maunaloa. **b**, Temporal variations in Nb/Y for Kīlauea lavas (see key for symbols), and variations in ground deformation and seismic activity at Maunaloa. The Nb/Y ratio tracks mantle-derived changes in the composition of the parental magma delivered to the volcano. The relative change in distance across Moku‘āweoweo between stations MOKP and MLSP is shown. The scale bar (see key) indicates a 5-cm change in MOKP-MLSP distance (Thelen et al., 2017), which was determined by electronic distance measurements (EDM) from 1984 to 2004 (green line) and by GPS from 2000 to 2022 (blue line, solid for continuous data). Earthquakes (M1.7 or greater) for Maunaloa with hypocenters near Moku‘āweoweo (dashed rectangle in **a**) are shown as yearly averages (orange bars) and cumulative numbers (brown line). Scale bars (see key) indicate counts of annual or cumulative earthquakes. Literature data sources for Nb/Y (collected by X-ray

fluorescence spectrometry, XRF), ground deformation, and seismic activity are listed in the **Supplementary Materials**. The error bar (2SD) for Nb/Y is shown.

Fig. 2. Compositional variations of lavas from Kīlauea and Maunaloa. **a**-**b**, The Pb, Sr, and Nd isotope ratios define systematic trends with rare overlap between the two volcanoes. End-member mantle source components for Kīlauea (K) and Maunaloa (M) are based on the average of the most extreme lavas. The isotopic composition of the shared mantle source (S) is estimated from the intersection of the best-fit lines (dashed with the 95% confidence intervals shown in gray) through Kīlauea and Maunaloa lavas. Mixing lines with 10% increments (small gray circles) between magmas derived from the K and M source components are shown. Concentrations of Pb (from an assumed Ce/Pb~30), Sr, and Nd for the mixing end members are from: (1) an average of sample HI10-2 for M and (2) the Kil1919 reference material for K. Inset in **a** illustrates the temporal variations in $^{206}Pb/^{204}Pb$ and $^{87}Sr/^{86}Sr$. **c**-**e**, Trace element ratios of Kīlauea and Maunaloa lavas are distinct except for the Maunaloa-like lavas from Uēkahuna bluff (gray fields). **f**, Histogram of Nb/Y for lavas from Kīlauea averaged with an equal temporal sampling density (**Supplementary Materials**) compared to the total range for Maunaloa since 1843. Literature data sources are listed in the **Supplementary Materials** (**c**, **e**, and **f**, data collected by quadrupole inductively coupled plasma mass spectrometry, ICPMS; **d**, data collected by XRF). Error bars (2SD) are shown unless they are smaller than the size of the symbols.

Fig. 3. Temporal variations in lava chemistry at Kīlauea and Maunaloa. **a**-**c**, The $^{206}Pb/^{204}Pb$, $^{87}Sr/^{86}Sr$, and Ce/Yb ratios define systematic trends with rare overlap between these volcanoes.

Inferred $^{206}Pb/^{204}Pb$ and $^{87}Sr/^{86}Sr$ ratios for the shared mantle source (dashed lines in **a** and **b**) are based on the intersection of the best-fit trends (including the 95% confidence intervals in the gray fields) from **Fig. 2a**. Samples that approach the shared source and the end-member mantle source components for Kīlauea (K) and Maunaloa (M) are marked by gray ovals in **a** and **b**. The relative effect of variable melt fraction on Ce/Yb is shown in **c**. Literature data sources are listed in the **Supplementary Materials** (**c**, collected by ICPMS). For clarity, Pu‘u‘ō‘ō lavas are plotted as the average of 2-year periods, as described in the **Supplementary Materials**. Error bars (2SD) are shown unless they are smaller than the size of the symbols. Keys to the symbols are shown in **Fig. 2**. **d**, Variations in lava eruption rate at Kīlauea and Maunaloa, calculated as described in the **Supplementary Materials**. Fields emphasize the highest and lowest eruption ratios for Maunaloa and Kīlauea, respectively. No written records exist for eruptions at Kīlauea prior to 1823 or Maunaloa prior to 1843.

Fig. 4. Model for short-term changes in the pathways of melt transport beneath Kīlauea and Maunaloa. Melt is generated within the Hawaiian mantle plume (asthenosphere), which is compositionally heterogeneous (blobs). Each volcano taps melt from their respective end-member sources, which are inferred to lie separately within the typical melting region of each volcano. A third, compositionally distinct mantle source—the shared component—is likely located between these volcanoes. Melt from the shared mantle source is diverted alternately to Maunaloa (**a**) or Kīlauea (**b**) on a timescale of decades. The mantle lithosphere includes a break in scale. **a**, Melt transport pathways inferred for both the early 19th century and the mid-20th to early 21st centuries. **b**, Melt transport pathways inferred for the late 19th to early 20th centuries.

Journal of Petrology, 2024, **65**, egae121. https://doi.org/10.1093/petrology/egae121

Supplementary Materials

Awakening of Maunaloa linked to melt shared from Kīlauea's mantle source

Aaron J. Pietruszka[1], Daniel E. Heaton[2], Jared P. Marske[3], Marc D. Norman[4], Mahinaokalani G. Robbins[1], Reed B. Mershon[1], Kendra J. Lynn[5], Drew T. Downs[5], Arron R. Steiner[6], J. Michael Rhodes[7], Michael O. Garcia[1]

[1]Department of Earth Sciences, University of Hawai'i at Mānoa, Honolulu, HI 96822, USA

[2]Oregon State University, College of Earth, Ocean, and Atmospheric Sciences, Corvallis, OR 97331, USA

[3]Department of Geology, Occidental College, Los Angeles, CA 90041, USA

[4]Research School of Earth Sciences, Australian National University, Canberra ACT 2601, Australia

[5]U.S. Geological Survey, Hawaiian Volcano Observatory, Hilo, HI 96720, USA

[6]School of the Environment, Washington State University, Pullman, Washington 99163, USA

[7]Department of Geosciences, University of Massachusetts, Amherst, MA 01003, USA

*Corresponding author (apietrus@hawaii.edu)

Description of the dataset

We present a comprehensive dataset of trace element abundances and high-precision Pb, Sr, and Nd isotope ratios for lavas from Kīlauea (~1820-1982) and Maunaloa (~1843-1984), and older lavas from Maunaloa (~140-2,580 yr before present, BP). Many of these samples were analyzed in previous studies (Rhodes & Hart, 1995; Pietruszka & Garcia, 1999; Garcia et al., 2003; Wanless et al., 2006; Marske et al., 2007, 2008; Weis et al., 2011; Greene et al., 2013; Pietruszka et al., 2013, 2015; Rhodes, 2015; Pietruszka et al., 2018, 2019, 2021), but some of the sample suites lack key chemical and/or isotopic data. This issue is rectified with new data, as described in detail below. Additionally, major and trace element abundances are presented for

lava samples from recent eruptions of each volcano (**Supplementary Table S1**), with three from Kīlauea's summit (2016, 2017, and 2021) and one from Maunaloa (2022). This dataset is augmented by previous studies of lavas from the Pu‘u‘ō‘ō rift eruption of Kīlauea (Garcia et al., 2021) and the ~1000-1400 CE lavas from the wall of Kīlauea‘s summit caldera (Kaluapele) at Uēkahuna bluff (Marske et al., 2007; Pietruszka et al., 2013).

A major goal of this study is to infer the temporal changes in the composition of the mantle-derived magma delivered to Kīlauea and Maunaloa. Thus, we use tracers of lava chemistry that are insensitive to the effects of magmatic differentiation (**Fig. 2**), including Pb, Sr, and Nd isotope ratios and ratios of incompatible trace elements. Furthermore, it is important to avoid using samples that are known to be significantly affected by crustal contamination or mixing with older, stored magma within the volcano's plumbing system. For example, the Pu‘u‘ō‘ō eruption was located on the East Rift Zone (ERZ) of Kīlauea (**Fig. 1a**), and was supplied by magma from the volcano's summit reservoir (Garcia et al., 2021). Pu‘u‘ō‘ō lavas display a relatively wide compositional range due to (1) an early period of mixing from 1983 to early 1985 between summit-derived magma and a differentiated, rift-stored magma from the 1960s (Garcia et al., 1989, 1992, 1996; Pietruszka et al., 2018) and (2) the gradual flushing of 1982-era summit-derived magma (via the ERZ) that was not complete until mid-1988 (Pietruszka et al., 2018). The Pu‘u‘ō‘ō eruption was also punctuated by three brief uprift eruptions in 1997, 2007, and 2011 (Garcia et al., 2021). Lavas from two of these eruptions (1997 and 2011) display chemical signs of mixing with a differentiated, rift-stored magma from the 1960s (Walker et al., 2019). Thus, Pu‘u‘ō‘ō lavas that erupted from 1983 to July 1988, and lavas from the uprift eruptions in 1997 and 2011, are excluded from the figures and discussion (except for **Fig. 2f**) because they do not

represent mantle-derived magmas. Other samples from both Kīlauea and Maunaloa that are excluded from further consideration are described below.

Lava samples from Kīlauea's summit and rift zones (~1820 to 1954)

High-precision Pb isotope ratios of 28 lava samples that erupted from Kīlauea's summit and rift zones between ~1820 and 1954 were previously reported by Pietruszka et al. (2019). The Sr and Nd isotope ratios were measured by thermal ionization mass spectrometry (TIMS) at San Diego State University (SDSU) or the U.S. Geological Survey (USGS) in Denver (Sr), and multiple-collector inductively coupled plasma mass spectrometry (MC-ICPMS) at SDSU (Nd). The average Sr and Nd isotope ratios of these samples, including the Kil1919 reference material, are presented in **Supplementary Table S2**. Individual replicate measurements of $^{87}Sr/^{86}Sr$ for each sample are presented in **Supplementary Table S3**. Kil1919 was collected from the same lava flow at the summit of Kīlauea as the USGS reference materials, BHVO-1 and BHVO-2. A subset of these samples from the summit (n=11, including Kil1919 and BHVO-2) and rift zones (n=5) was analyzed for trace element abundances by quadrupole inductively coupled plasma mass spectrometry (ICPMS) at the Australian National University (ANU) or Washington State University (WSU). The ICPMS trace element abundances of these samples are presented in **Supplementary Table S4** (summit) and **Supplementary Table S5** (rift zones). These data supplement the published ICPMS trace element abundances of summit lavas (Pietruszka & Garcia, 1999) from this time period (n=24), including six samples that were reanalyzed in this study (1832, 1885-2, 1917, 1918-1919, Kil1919 and 1921-4). Detailed information on the eruptive history and locations of the summit and rift zone samples, and their previously reported major element abundances by X-ray fluorescence spectrometry (XRF) or electron microprobe are summarized by Garcia et al. (2003) and Pietruszka et al. (2019). New XRF major element

abundances for seven additional samples from the 1919-1920 Maunaiki eruption (**Fig. 1a**) along the Southwest Rift Zone (SWRZ) of Kīlauea are presented in **Supplementary Table S6**, which includes new XRF trace element abundances for these Maunaiki lavas, another sample from this eruption (previously analyzed by Pietruszka et al. (2019) for major element abundances), and three additional rift zone lavas that erupted in 1823 (SWRZ), 1868 (SWRZ), and 1923 (ERZ). All XRF analyses were performed at the University of Massachusetts (UM).

The Pb isotope ratios of seven Kīlauea summit lavas that erupted from 1912 to 1954 are unusually variable with elevated $^{207}Pb/^{204}Pb$ (95-TAJ-3, 95-TAJ-15, 1918-1919, KS11-2, 95-TAJ-9, 26-Jun-1952, 1954-2). These anomalous signatures are thought to result from the contamination of mantle-derived magmas with the ~110 Ma Pacific oceanic crust that underlies the Island of Hawai‘i (Pietruszka et al., 2019). The $^{87}Sr/^{86}Sr$ ratios of two groups of these samples (two different samples of the 1918-1919 summit lava flow, 1918-1919 and KS11-2, and two separate analyses of sample 95-TAJ-9 from the 1923 summit eruption) are also somewhat variable (**Supplementary Table S2**). The specific origin of these differences in $^{87}Sr/^{86}Sr$ (~0.00002 to 0.00006) is unknown, but may be related to a disruption of Kīlauea's magmatic plumbing system during a period of low magma supply prior to the 1924 collapse of Halema‘uma‘u lava lake and explosive eruption (Pietruszka et al., 2019). Of these samples, the $^{87}Sr/^{86}Sr$ ratios of KS11-2 and both analyses of 95-TAJ-9 seem to be anomalously high compared to the overall temporal trend. The Sr isotope ratios of these anomalous samples and those listed above with elevated $^{207}Pb/^{204}Pb$—also identified in **Supplementary Table S2**—are not plotted on the figures or used in the interpretation of mantle processes.

Lava samples from Kīlauea's summit (1959 to 1982)

High-precision Pb, Sr, and Nd isotope ratios of 25 lava samples that erupted from Kīlauea's summit between 1959 and 1982 were previously reported by Pietruszka et al. (2015, 2018). A subset of these samples (n=8) was analyzed for trace element abundances by ICPMS at WSU (**Supplementary Table S4**). These data supplement the published ICPMS trace element abundances of summit lavas (Pietruszka & Garcia, 1999) from this time period (n=15), including one sample that was reanalyzed in this study (1982S-12). Detailed information on the eruptive history and locations of these samples, and their previously reported major and trace element abundances are summarized by Pietruszka & Garcia (1999), Garcia et al. (2003), and Pietruszka et al. (2015).

Lava samples from Kīlauea's rift zones (1961 to 1979)

High-precision Pb, Sr, and Nd isotope ratios of 27 lava samples that erupted from Kīlauea's rift zones between 1961 and 1979 were previously reported by Pietruszka et al. (2018). A subset of these samples (n=24) was analyzed for trace element abundances by ICPMS at ANU (**Supplementary Table S5**). Detailed information on the eruptive history and locations of these samples, and their previously reported XRF major and trace element abundances are summarized by Pietruszka et al. (2018). The sample from Kīlauea's 1977 ERZ eruption (KL77-11) is excluded from the figures and further discussion because it likely experienced a relatively long (>10 yr) period of rift storage (Pietruszka et al., 2018).

Lava samples from Maunaloa (1843 to 1984)

High-precision Pb, Sr, and Nd isotope ratios of 20 lava samples that erupted from Maunaloa between 1843 and 1984 were previously reported by Wanless et al. (2006) and Weis et al. (2011). One of these samples (ML-129) from the 1940 eruption (Weis et al., 2011) has an anomalously

low $^{206}Pb/^{204}Pb$ ratio (a large difference of ~0.2 compared to typical Maunaloa lavas), and is not considered further. All of these samples, and many others from this time period, were previously analyzed for their major element abundances by XRF (Rhodes & Hart, 1995; Wanless et al., 2006; Rhodes, 2015). Selected XRF trace element abundances for most of the samples with Pb, Sr, and Nd isotope ratios (n=16) and many others from this time period are published by Rhodes & Hart (1995) and Wanless et al. (2006); trace element abundances for the final four samples with Pb, Sr, and Nd isotope ratios were measured by XRF at UM (**Supplementary Table S7**). Only two of the samples with Pb, Sr and Nd isotope ratios—both from the submarine radial vents of the 1877 eruption—were previously analyzed for trace element abundances by ICPMS (Wanless et al., 2006). New trace element abundances for a sample from the 1877 eruption and four samples from the 1859 eruption by ICPMS at ANU (including new major and trace element abundances by XRF at UM) are presented in **Supplementary Table S8**. Five additional lava samples that erupted from Maunaloa between 1843 and 1984 (the H10 series of samples) were analyzed for major element abundances by XRF at UM, trace element abundances by ICPMS at ANU, and high-precision Pb, Sr, and Nd isotope ratios at SDSU (**Supplementary Table S9**). Individual replicate measurements of $^{87}Sr/^{86}Sr$ for each H10 sample are presented in **Supplementary Table S10**.

Older lava samples from Maunaloa

High-precision Pb, Sr, and Nd isotope ratios of 12 older lava samples erupted from Maunaloa between ~140 and 2,580 yr before present (Rhodes, 2015) were previously reported by Marske et al. (2007). These samples plus an additional 20 from this time period were analyzed for selected trace element abundances by XRF at UM (**Supplementary Tables S7 and S8**). A subset of the samples (n=17) with Pb, Sr, and Nd isotope ratios and/or trace element abundances by XRF were

analyzed for trace element abundances by ICPMS at ANU (**Supplementary Table S8**). All of these samples, and many others from this time period, were previously analyzed for their major element abundances by XRF (Marske et al., 2007; Rhodes, 2015).

Analytical methods

The Pb, Sr, and Nd isotope analytical methods, including estimates of precision and all data for reference materials analyzed during the course of this study, are the same as described by Pietruszka et al. (2018). All literature isotopic data have been corrected relative to the same values for the SRM981 Pb (Galer and Abouchami, 1998), SRM987 Sr ($^{87}Sr/^{86}Sr$=0.710250), and La Jolla Nd ($^{143}Nd/^{144}Nd$=0.511844) standards for direct comparison with the data presented in this study. Measurements of trace element abundances by ICPMS at ANU were performed using the methods described by Pietruszka et al. (2013), and references therein.

Measurements of trace element abundances at WSU were performed using an Agilent 7700 ICPMS. Samples were powdered in agate, weighed (0.2000±0.0005 g), digested in a mixture of concentrated HCl (2 mL), HNO_3 (2 mL), $HClO_4$ (2 mL), and HF (6 mL), and dried. The sample was treated with a second dose of $HClO_4$ (2 mL) and dried. A clear solution was obtained in a mixture of 18MΩ water (10 mL), concentrated HNO_3 (3 mL), H_2O_2 (0.35 mL), and 0.1 mL of concentrated HF. Each sample was spiked with an In-Re-Rh-Ru internal standard, diluted with 18MΩ water to 60 g, and homogenized. The ICPMS analyses were calibrated against two USGS basalt reference materials, BCR-2 and BHVO-2, that were prepared using the same procedure as the samples. The calibration values for BCR-2 and BHVO-2 are listed in **Supplementary Table S11**.

Data for ICPMS reference materials analyzed during this study (Kil1919, BHVO-2, and Kil93), including estimates of precision, are presented in **Supplementary Table S11**. Kil1919

and BHVO-2 are both whole-rock powders prepared from the same 1919 summit lava flow of Kīlauea, and are expected to be essentially identical for abundances of incompatible trace elements. Kil93 is a whole-rock powder prepared from a Pu‘u‘ō‘ō (Kīlauea) lava that was collected on May 10, 1993. Due to differences in the method of instrument calibration, a correction for interlaboratory bias is recommended to compare the trace element abundances more accurately between WSU and ANU. The suggested correction factors, based on the measured differences in the reference materials, are listed in **Supplementary Table S11**. The "WSU99" correction factors apply to the ICPMS trace element abundances of Kīlauea summit lavas from Pietruszka & Garcia (1999). The "WSU2020s" correction factors apply to the results for recent Kīlauea (2016, 2017, and 2021) and Maunaloa (2022) lavas in **Supplementary Table S1** and Kīlauea summit lavas (1832-1982) in **Supplementary Table S4**. These correction factors were only applied to the ICPMS data shown on the figures; the data are reported as measured. The major and selected trace element (Nb, Zr, Y, Sr, Rb, Zn, Ni, Cr, V, and, in some cases, Ba) abundances of the samples (and all of the literature data) were measured by XRF using the methods described by Rhodes & Vollinger (2004).

Sources of geophysical data

Data for ground deformation and seismic activity at Maunaloa is shown in **Fig. 1b**. The relative change in distance across Moku‘āweoweo between the MOKP and MLSP stations (**Fig. 1a**) was determined by electronic distance measurements (EDM) from 1984 to 2004 (Thelen et al., 2017) and by GPS from 2000 to 2022 (HVO, USGS, Hawai‘i GPS Network, 2000a, 2000b). Earthquake counts with hypocenters near Moku‘āweoweo (dashed rectangle in **Fig. 1a**) were filtered for M1.7 or greater [the minimum consistently detectable magnitude since ~1984 based

on Thelen et al. (2017)] from the comprehensive catalog of the U.S. Geological Survey (USGS, Earthquake Hazards Program, 2017). These data sources are continuously updated by the USGS.

Histogram of Kīlauea lava chemistry

The distribution of lava chemistry at Kīlauea is illustrated in **Fig. 2f**. This histogram of Nb/Y (collected by ICPMS) compares all lavas in the comprehensive dataset (described above) from Kīlauea's summit (~1820-2021 and the ~1000-1400 CE lavas from Uēkahuna bluff) and rift zones (1823-2018) with the total range for Maunaloa lavas (1843-2022). However, some Kīlauea eruptions (e.g., Pu‘u‘ō‘ō) were more frequently sampled and analyzed (weekly to monthly) than many others that may only have a single analysis. To avoid skewing the histogram, we determined the average temporal spacing for Kīlauea eruptions that were sampled and analyzed from 1918-1919 (the earliest overflow of Halema‘um‘au lava lake onto the caldera floor that remains exposed) to September 1982 (the last eruption prior to the start of the Pu‘u‘ō‘ō). Samples from the Maunaulu eruption were divided into two groups (1969-1971 and 1972-1974), which are separated by an eruptive pause. Samples from the paired summit-rift eruptions in September 1971 and July 1974 were each treated as a single group. The total of 36 eruptions from 1918-1919 to September 1982 represent an average of ~1.8 yr between sampled and analyzed eruptions. Thus, the entire dataset for Nb/Y from ~1820 to 2021 (including Pu‘u‘ō‘ō) was averaged with a 2-yr filter both forwards (to 2021) and backwards (to ~1820) from a starting window of 1981 to 1982. The exact dates of the 1918-1919 summit eruption are unknown, but the histogram remains the same if it is included with either the 1917 to 1918 or 1918 to 1919 time units. Overall, this approach to estimate the distribution in Nb/Y for Kīlauea lavas results in 27 time units with data for summit eruptions, 18 for the Pu‘u‘ō‘ō eruption, and 14 for other rift eruptions. The average Nb/Y ratio of each time unit is plotted separately for summit and rift

lavas in **Fig. 2f**. Each of the 24 lava samples from Uēkahuna bluff are plotted separately because the timing of these eruptions is unknown.

Calculation of eruption rates

Eruption rates at Kīlauea (1924-2023) and Maunaloa (1843-2022) were calculated using best-fit lines on plots of the cumulative volume of lava erupted over time (**Supplementary Fig. S1**). Eruption information, including the lava volume estimates, are from Mulliken et al. (2024). The slope of the line defined by a series of eruptions on this plot indicates the average rate of eruption for the time period. The eruption rates shown on **Fig. 3d** were determined from the best-fit slopes on **Supplementary Fig. S1** and other information for Kīlauea prior to 1924, as follows.

From ~1823 to 1924, volcanic activity at Kīlauea was dominated by a lava lake within the caldera (Kaluapele) or Halemaʻumaʻu (**Fig. 1a**) alone since the mid-19th century. Major collapses of the caldera in 1832, 1840, and 1868, and its subsequent refilling by lava lake overflows makes it impossible to estimate eruption rates at Kīlauea prior to 1924 using modern lava flow maps. Eruption rates of ~0.1 km^3/yr from 1823 to 1840 and ~0.01 km^3/yr from 1840 to 1924 were estimated by Pietruszka & Garcia (1999) using contemporaneous maps and descriptions of eruptive behavior. The eruption rate at Kīlauea reached a minimum after the collapse of Halemaʻumaʻu lava lake in 1924 (Pietruszka & Garcia, 1999), and remained low (~0.003 km^3/yr based on a best-fit line with an R^2 value of ~0.99) until ~1954 (**Supplementary Fig. S1a**). This includes the longest quiescent period (1934-1952) for Kīlauea since the start of written records in ~1823, and the subsequent two summit eruptions in 1952 and 1954. The 1955 rift eruption was relatively large, and marked a switch to more frequent eruptions at the volcano's summit (n=10 until 1982), along the rift zones (n=19), or both (n=2). Major rift eruptions occurred from 1969 to 1972 at Maunaulu, 1983 to 2018 at Puʻuʻōʻō, and in 2018, on

the lower ERZ (LERZ), mostly from Ahuʻailāʻau (**Fig. 1a**). The eruption rate at Kīlauea was higher from ~1955 to 1982 (~0.036 km^3/yr based on a best-fit line with an R^2 value of ~0.91), which was the last summit eruption prior to the start of the Puʻuʻōʻō eruption in 1983. The eruption rate from the start of the Puʻuʻōʻō eruption in 1983 to the end of the 2018 LERZ eruption (~0.15 km^3/yr) is estimated from the total volume of lava erupted during this period (~5.5 km^3). Kīlauea displayed a systematic variation in eruption rate during the Puʻuʻōʻō eruption (Wolfe et al., 1987; Dvorak & Dzurisin, 1993; Anderson & Poland, 2016): (1) ~0.12 km^3/yr from 1983 to 1984, (2), ~0.12 km^3/yr from 2000 to 2001, (3) ~0.16 km^3/yr from 2005 to 2006 during the mantle-derived surge in magma supply from ~2003 to 2007 (Poland et al., 2012), and (4) ~0.07 km^3/yr from 2011 to 2012. However, we use the long-term average eruption rate from 1983 to 2018—including both the Puʻuʻōʻō and 2018 LERZ eruptions—to be consistent with the estimates from the early 19th to mid-20th century. No eruptions occurred at Kīlauea between the end of the 2018 LERZ eruption and the start of the 2020 summit eruption within Halemaʻumaʻu. The cumulative volume of lava erupted from 2020 to 2023 can be fit (R^2=0.94) with an eruption rate of ~0.061 km^3/yr, which is more than a factor of ~2 lower than the average rate from 1983 to 2018. However, this estimate is likely affected by an unusually large amount of magma intrusion and storage following the 2018 collapse of Kaluapele. Instead, a higher estimate of ~0.093 km^3/yr is shown on **Fig. 3d**. This value was derived from the volume erupted at the volcano's summit during the sustained Halemaʻumaʻu eruption from September 2021 to December 2022 (~437 days), when the amount of deformation and magma storage was low (M. Poland, personal communication, 2024). The most recent Kīlauea eruptions on the SWRZ and ERZ in 2024 were not included in this analysis because no lava volume estimates are yet available, but both eruptions were small.

The plot of cumulative volume erupted over time at Maunaloa (**Supplementary Fig. S1b**) reveals three distinct periods of decreasing slope due to a decline in the rate of eruption from ~1843 to 2022: a maximum of ~0.062 km^3/yr from 1843 to 1890 (R^2=0.95), ~0.024 km^3/yr from 1890 to 1950 (R^2=0.95), and a minimum of ~0.006 km^3/yr from 1950 to 2022 (R^2=0.86). Unlike Kīlauea, however, there are fewer volcanological clues to these changes in eruption rate and it is not possible to unambiguously assign eruptions near each of the two changes in slope to a particular period. Instead, the eruptions included in each period were selected to maximize the R^2 value of the best-fit lines. These estimates are similar to Lockwood and Lipman (1987), who obtained average eruption rates of ~0.05 km^3/yr from 1843 to 1876 and ~0.02 km^3/yr from 1887 to 1984.

SUPPLEMENTARY REFERENCES

Anderson, K.R. & Poland, M.P. (2016). Bayesian estimation of magma supply, storage, and eruption rates using a multiphysical volcano model: Kīlauea Volcano, 2000–2012. *Earth and Planetary Science Letters* **447**, 161-171. https://doi.org/10.1016/j.epsl.2016.04.029.

Galer, S.J.G. & Abouchami, W. (1998). Practical application of lead triple spiking for correction of instrumental mass discrimination. *Mineralogical Magazine* **62A**, 491-492.

Garcia, M.O., Ho, R.A., Rhodes, J.M. & Wolfe, E.W. (1989). Petrologic constraints on rift-zone processes: results from episode 1 of the Pu‘u ‘Ō‘ō eruption of Kīlauea Volcano, Hawai‘i. *Bulletin of Volcanology* **52**, 81-96.

Garcia, M.O., Rhodes, J.M., Wolfe, E.W., Ulrich, G.E. & Ho, R.A. (1992). Petrology of lavas from episodes 2-47 of the Pu‘u ‘Ō‘ō eruption of Kīlauea Volcano, Hawai‘i: evaluation of magmatic processes. *Bulletin of Volcanology* **55**, 1-16.

Garcia, M.O., Rhodes, J.M., Trusdell, F.A. & Pietruszka, A.J. (1996). Petrology of lavas from the Pu‘u ‘Ō‘ō eruption of Kīlauea Volcano: III. The Kūpaianaha episode (1986-1992). *Bulletin of Volcanology* **58**, 359-379.

Garcia, M.O., Pietruszka, A.J. & Rhodes, J.M. (2003). A petrologic perspective of Kīlauea Volcano’s summit magma reservoir. *Journal of Petrology* **44**, 2313-2339.

Garcia, M.O., Pietruszka, A.J., Norman, M.D. & Rhodes, J.M. (2021). Kīlauea's Pu‘u ‘Ō‘ō eruption (1983-2018): a synthesis of magmatic processes during a prolonged basaltic event. *Chemical Geology* **581**, 120391. https://doi.org/10.1016/j.chemgeo.2021.120391.

HVO, USGS (2000a). Hawai‘i GPS Network - MLSP-Mauna Loa Summit P.S., The GAGE Facility operated by EarthScope Consortium, GPS/GNSS Observations Dataset. https://doi.org/10.7283/T5K64G9H.

HVO, USGS (2000b). Hawai‘i GPS Network - MOKP-Moku‘āweoweo P.S., The GAGE Facility operated by EarthScope Consortium, GPS/GNSS Observations Dataset. https://doi.org/10.7283/T5TQ5ZS9.

Lockwood J.P. & Lipman, P.W. (1987). Holocene eruptive history of Mauna Loa volcano. In: Decker, R.W., Wright, T.L. & Stauffer, P.H. (eds), *Volcanism in Hawai‘i*, U.S. Geological Survey, Professional Paper **1350**, 509-536.

Mulliken, K.M., Kauahikaua, J.P., Swanson, D.A., & Zoeller, M.H. (2024). Chronology of recent volcanic activity on the Island of Hawai‘i, Hawai‘i. *U.S. Geological Survey Data Release*. https://doi.org/10.5066/P9V3NQYB.

Pietruszka, A.J., Marske, J.P., Heaton, D.E., Garcia, M.O. & Rhodes, J.M. (2018). An isotopic perspective into the magmatic evolution and architecture of the rift zones of Kīlauea Volcano. *Journal of Petrology* **59**, 2311-2352. https://doi.org/10.1093/petrology/egy098.

Pietruszka, A.J., Heaton, D.E., Garcia, M.O. & Marske, J.P. (2019). Explosive summit collapse of Kīlauea Volcano in 1924 preceded by a decade of crustal contamination and anomalous Pb isotope ratios. *Geochimica et Cosmochimica Acta* **258**,120-137. https://doi.org/10.1016/j.gca.2019.05.029.

Pietruszka A.J., Garcia, M.O. & Rhodes, J.M. (2021). Accumulated Pu‘u ‘Ō‘ō magma fed the voluminous 2018 rift eruption of Kīlauea Volcano: evidence from lava chemistry. *Bulletin of Volcanology* **83**, 59. https://doi.org/10.1007/s00445-021-01470-3.

Rhodes, J.M. (2015). Major-element and isotopic variations in Mauna Loa magmas over 600 ka: implications for magma generation and source lithology as Mauna Loa transits the Hawaiian plume. In: Carey, R.J., Cayol, V., Poland, M.P. & Weis, D. (eds), *Hawaiian Volcanoes: From Source to Surface*. *American Geophysical Union, Geophysical Monograph* **208**, pp. 59-78.

Rhodes, J.M. & Vollinger, M.J. (2004). Composition of basaltic lavas sampled by phase-2 of the Hawai‘i Scientific Drilling Project: geochemical stratigraphy and magma types, *Geochemistry, Geophysics, Geosystems* **5**, Q03G13. https://doi:10.1029/2002GC000434.

USGS, Earthquake Hazards Program (2017). Advanced National Seismic System (ANSS) Comprehensive Catalog of Earthquake Events and Products, Various. https://doi.org/10.5066/F7MS3QZH.

Walker, B.H., Garcia, M.O. & Orr, T.R. (2019). Petrologic insights into rift zone magmatic interactions from the 2011 eruption of Kīlauea Volcano, Hawai‘i. *Journal of Petrology* **60**, 2051-2076. https://doi.org/10.1093/petrology/egz064.

Wanless, V.D., Garcia, M.O., Trusdell, F.A., Rhodes, J.M., Norman, M.D., Weis, D., Fornari, D.J., Kurz, M.D. & Guillou, H. (2006). Submarine radial vents on Mauna Loa Volcano, Hawai‘i. *Geochemistry, Geophysics, Geosystems* **7**, Q05001. https://doi.org/10.1029/2005GC001086.

Wolfe, E.W., Garcia, M.O., Jackson, D.B., Koyanagi, R.Y., Neal, C.A. & Okamura, A.T. (1987). The Puu Oo eruption of Kilauea Volcano, Episodes 1-20, January 3, 1983, to June 8, 1984. In: Decker, R.W., Wright, T.L. & Stauffer, P.H. (eds), *Volcanism in Hawai‘i*, U.S. Geological Survey, Professional Paper **1350**, 471-508.

Supplementary Figure and Table Captions

Supplementary Fig. S1. Cumulative volume of lava erupted for Kīlauea (1924 to 2023) and Maunaloa (1843 to 2022). The lava volume estimates are from the summary of Mulliken et al. (2024).

Supplementary Table S1. Major and trace element abundances of lava samples from recent eruptions of Kīlauea and Maunaloa

The Kīlauea samples were collected from the lava lake within Halemaʻumaʻu at the summit of the volcano in 2016, 2017, and 2021. The XRF major and trace element abundances of the 2016 and 2017 samples were presented by Pietruszka et al. (2021). The 2022 Maunaloa sample erupted from the volcano's Northeast Rift Zone (NERZ), and was collected at the flow front closest to Highway 200 by water quenching at ~1300 hrs (Hawaiian Standard Time) on December 5, 2022. The major and selected trace element abundances of the 2021 Kīlauea and 2022 Maunaloa lavas were measured by XRF at the University of Massachusetts (UM) using the methods of Rhodes & Vollinger (2004). $Fe_2O_3^*$ is total iron as Fe^{3+}. All four samples were analyzed for trace element abundances by ICPMS in solution mode at Washington State University (WSU) using methods described in the text. Data for ICPMS reference materials analyzed during the course of this study, including estimates of precision, are presented in **Supplementary Table S11**.

Supplementary Table S2. Sr and Nd isotope ratios for lava samples from Kīlauea's summit and rift zones (~1820 to 1954)

The samples were collected from the summit, Southwest Rift Zone (SWRZ), or East Rift Zone (ERZ) of Kīlauea, as described by Pietruszka et al. (2019). The Sr isotope ratios were measured by thermal ionization mass spectrometry (TIMS) at either San Diego State University (SDSU) or the U.S. Geological Survey (USGS) in Denver. The details of the Pb, Sr, and Nd isotope analytical methods, including estimates of precision and all data for reference materials analyzed during the course of this study, are the same as described by Pietruszka et al. (2018). The materials analyzed were volcanic glass (GL) or groundmass (GM) chips, or for Kil1919 only, a whole-rock powder (WR). The Pb isotope ratios from Pietruszka et al. (2019) are provided to unambiguously link the duplicate analyses with their Sr and Nd isotope ratios. The uncertainties for the average Sr isotope ratios are ±2SE (n>2) or the total range (n=2) of the replicate analyses of each sample. The individual Sr isotope ratios are presented in **Supplementary Table S3**. The ε_{Nd} values are calculated relative to $^{143}Nd/^{144}Nd=0.512638$ for $\varepsilon_{Nd}=0$.

Notes:

(a) The Sr isotope ratio of this sample was measured at the USGS.

(b) The Sr isotope ratio of this sample was measured at SDSU.

(c) Duplicate analysis from a separate split of the sample.

(d) Leached analysis from a separate split of the sample.

(e) Average Pb, Sr, and Nd isotope ratios for Kil1919 from this study and a previous study in the same laboratory by Marske et al. (2007).

(f) The Pb isotope ratios of this sample are anomalous (with high $^{207}Pb/^{204}Pb$) due to crustal contamination, as described by Pietruszka et al. (2019).

(g) Analyses of $^{87}Sr/^{86}Sr$ for different samples of this 1918-1919 lava flow are distinct at the ±2SD level.

(h) The duplicate analyses of $^{87}Sr/^{86}Sr$ for this sample are distinct at the ±2SD level.

Supplementary Table S3. Individual Sr isotope ratios for lava samples from Kīlauea's summit and rift zones (~1820 to 1954)

Supplementary Table S4. ICPMS trace element abundances for lavas from Kīlauea's summit (1832 to 1982)

The trace element abundances were measured by ICPMS in solution mode at WSU using methods described in the text. Data for ICPMS reference materials analyzed during the course of this study, including estimates of precision, are presented in **Supplementary Table S11**.

Supplementary Table S5. ICPMS trace element abundances for lavas from Kīlauea's rift zones (1823 to 1923)

The trace element abundances were measured by ICPMS, either in solution mode (Soln.) or as fused whole-rock powders by laser ablation (LA) at the Australian National University (ANU). The analytical method was described by Pietruszka et al. (2013) and references therein. The reported values by LA-ICPMS are the average of at least three measurements. Data for ICPMS reference materials analyzed during the course of this study, including estimates of precision, are presented in **Supplementary Table S11**.

Supplementary Table S6. XRF major and selected trace element abundances for lavas from Kīlauea's rift zones (1823 to 1923)

The major and selected trace element abundances were measured by XRF at UM using the methods of Rhodes & Vollinger (2004). $Fe_2O_3^*$ is total iron as Fe^{3+}. The major element abundances of four samples (1823SW-F, 1868SW, MI-07-02, and 25-Aug-23) are from Pietruszka et al. (2019).

Supplementary Table S7. XRF major and selected trace element abundances for lavas from Maunaloa

The major and selected trace element abundances were measured by XRF at UM using the methods of Rhodes & Vollinger (2004). $Fe_2O_3^*$ is total iron as Fe^{3+}.

Notes:

(a) Major element abundances from Rhodes (2015).

Supplementary Table S8. Major and trace element abundances for lavas from Maunaloa by XRF and ICPMS

The major and selected trace element abundances were measured by XRF at UM using the methods of Rhodes & Vollinger (2004). $Fe_2O_3^*$ is total iron as Fe^{3+}. The trace element abundances were measured by ICPMS in solution mode at ANU using the analytical method described by Pietruszka et al. (2013) and references therein. The reported values are a single ICPMS measurement, except for sample L88-29 (average of two analyses). Data for ICPMS reference materials analyzed during the course of this study, including estimates of precision, are presented in **Supplementary Table S11**.

Notes:

(a) Major element abundances from Marske et al. (2007).

Supplementary Table S9. Major (XRF) and trace element (ICPMS) abundances, and Pb, Sr, and Nd isotope ratios of lava samples from Maunaloa (1843 to 1984)

The samples were collected at the given coordinates (latitude and longitude) from the summit, radial vents, Northeast Rift Zone (NERZ), or Southwest Rift Zone (SWRZ) of Maunaloa. The major element abundances were measured by XRF at UM using the methods of Rhodes & Vollinger (2004). $Fe_2O_3^*$ is total iron as Fe^{3+}. The trace element abundances were measured as fused whole-rock powders by LA-ICPMS at ANU using the analytical method described by Pietruszka et al. (2013), and references therein. The reported values are the average of three ICPMS measurements. Data for ICPMS reference materials analyzed during the course of this study, including estimates of precision, are presented in **Supplementary Table S11**. The Pb, Sr, and Nd isotope ratios were measured in whole-rock chips by multiple-collector inductively coupled plasma mass spectrometry (MC-ICPMS) at SDSU (Pb and Nd) or by TIMS at the USGS (Sr). The details of the Pb, Sr, and Nd isotope analytical methods, including estimates of precision and all data for reference materials analyzed during the course of this study, are the same as described by Pietruszka et al. (2018). The Sr isotope ratios are the average of two or three replicates (see **Supplementary Table S10** for the individual $^{87}Sr/^{86}Sr$ ratios). The ε_{Nd} values are calculated relative to $^{143}Nd/^{144}Nd=0.512638$ for $\varepsilon_{Nd}=0$.

Supplementary Table S10. Individual Sr isotope ratios for lava samples from Maunaloa (1843 to 1984)

Supplementary Table S11. Trace element abundances for ICPMS reference materials

Figure 1

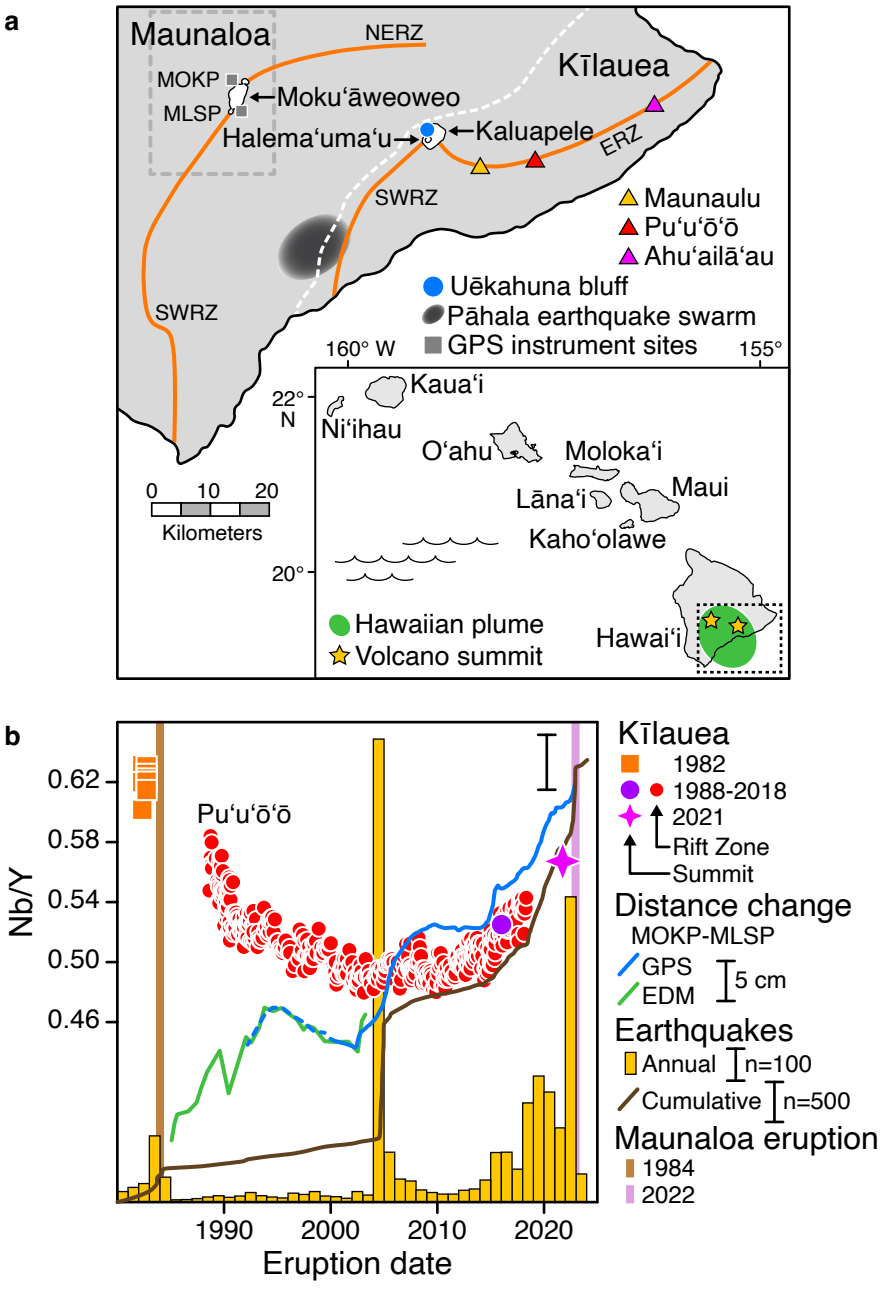
a
Maunaloa
NERZ
Kīlauea
MOKP
MLSP
Moku‘āweoweo
Halema‘uma‘u
Kaluapele
ERZ
SWRZ
SWRZ
Maunaulu
Pu‘u‘ō‘ō
Ahu‘ailā‘au
Uēkahuna bluff
Pāhala earthquake swarm
GPS instrument sites
160° W
155°
22° N
20°
Kaua‘i
Ni‘ihau
O‘ahu
Moloka‘i
Lāna‘i
Maui
Kaho‘olawe
Hawai‘i
0 10 20
Kilometers
Hawaiian plume
Volcano summit
b
Nb/Y
0.62
0.58
0.54
0.50
0.46
Pu‘u‘ō‘ō
1990
2000
2010
2020
Eruption date
Kīlauea
1982
1988-2018
2021
Rift Zone
Summit
Distance change
MOKP-MLSP
GPS
EDM
5 cm
Earthquakes
Annual
n=100
Cumulative
n=500
Maunaloa eruption
1984
2022

Figure 2

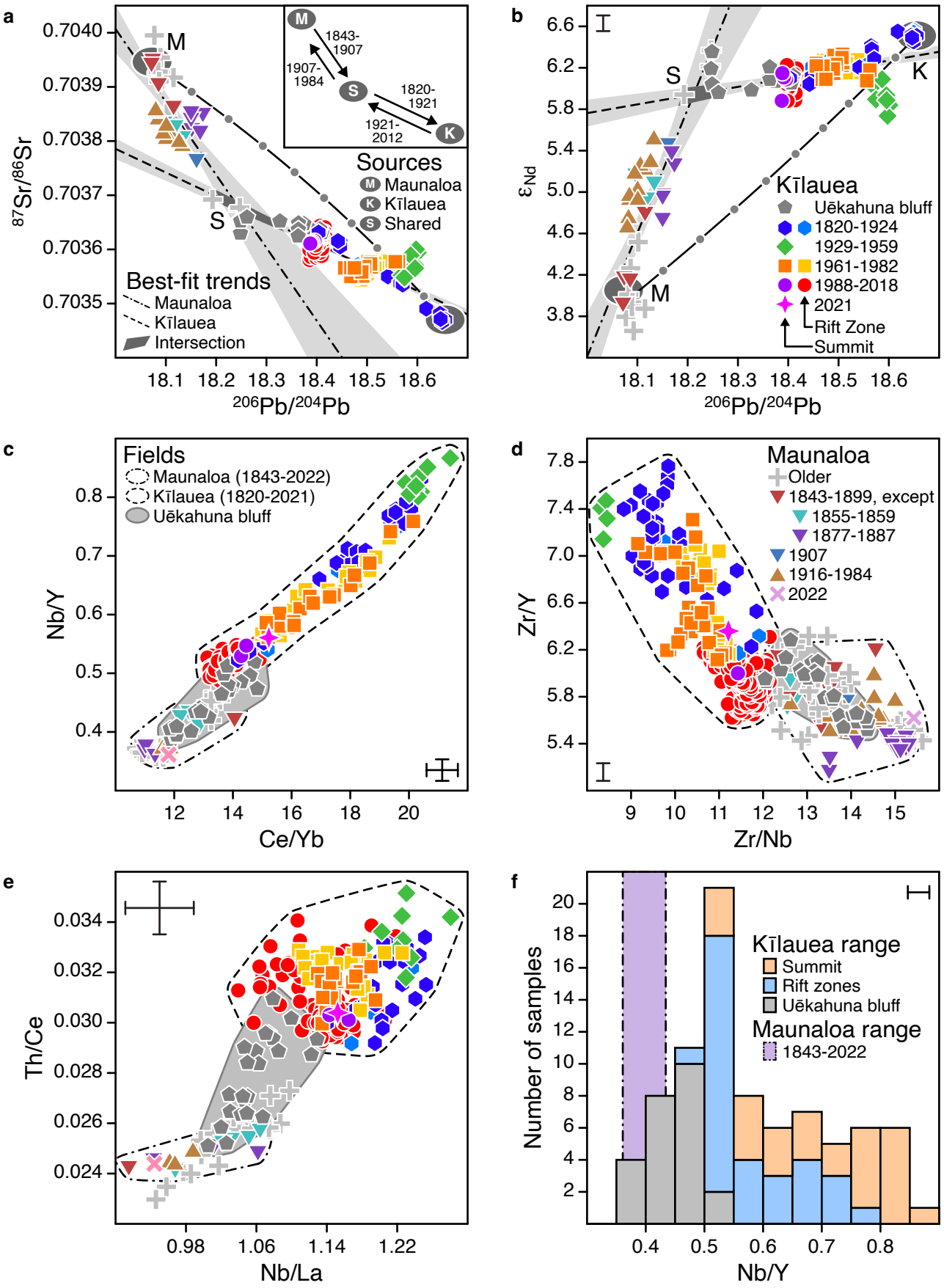
a
0.7040
0.7039
0.7038
0.7037
0.7036
0.7035
87Sr/86Sr
M
S
M
1843-
1907
1907-
1984
S
1820-
1921
1921-
2012
K
Sources
Maunaloa
Kīlauea
Shared
Best-fit trends
Maunaloa
Kīlauea
Intersection
18.1 18.2 18.3 18.4 18.5 18.6
206Pb/204Pb
b
6.6
6.2
5.8
5.4
5.0
4.6
4.2
3.8
εNd
S
K
M
Kīlauea
Uēkahuna bluff
1820-1924
1929-1959
1961-1982
1988-2018
2021
Rift Zone
Summit
18.1 18.2 18.3 18.4 18.5 18.6
206Pb/204Pb
c
Fields
Maunaloa (1843-2022)
Kīlauea (1820-2021)
Uēkahuna bluff
0.8
0.7
0.6
0.5
0.4
Nb/Y
12 14 16 18 20
Ce/Yb
d
Maunaloa
Older
1843-1899, except
1855-1859
1877-1887
1907
1916-1984
2022
7.8
7.4
7.0
6.6
6.2
5.8
5.4
Zr/Y
9 10 11 12 13 14 15
Zr/Nb
e
0.034
0.032
0.030
0.028
0.026
0.024
Th/Ce
0.98 1.06 1.14 1.22
Nb/La
f
20
18
16
14
12
10
8
6
4
2
Number of samples
Kīlauea range
Summit
Rift zones
Uēkahuna bluff
Maunaloa range
1843-2022
0.4 0.5 0.6 0.7 0.8
Nb/Y

Figure 3

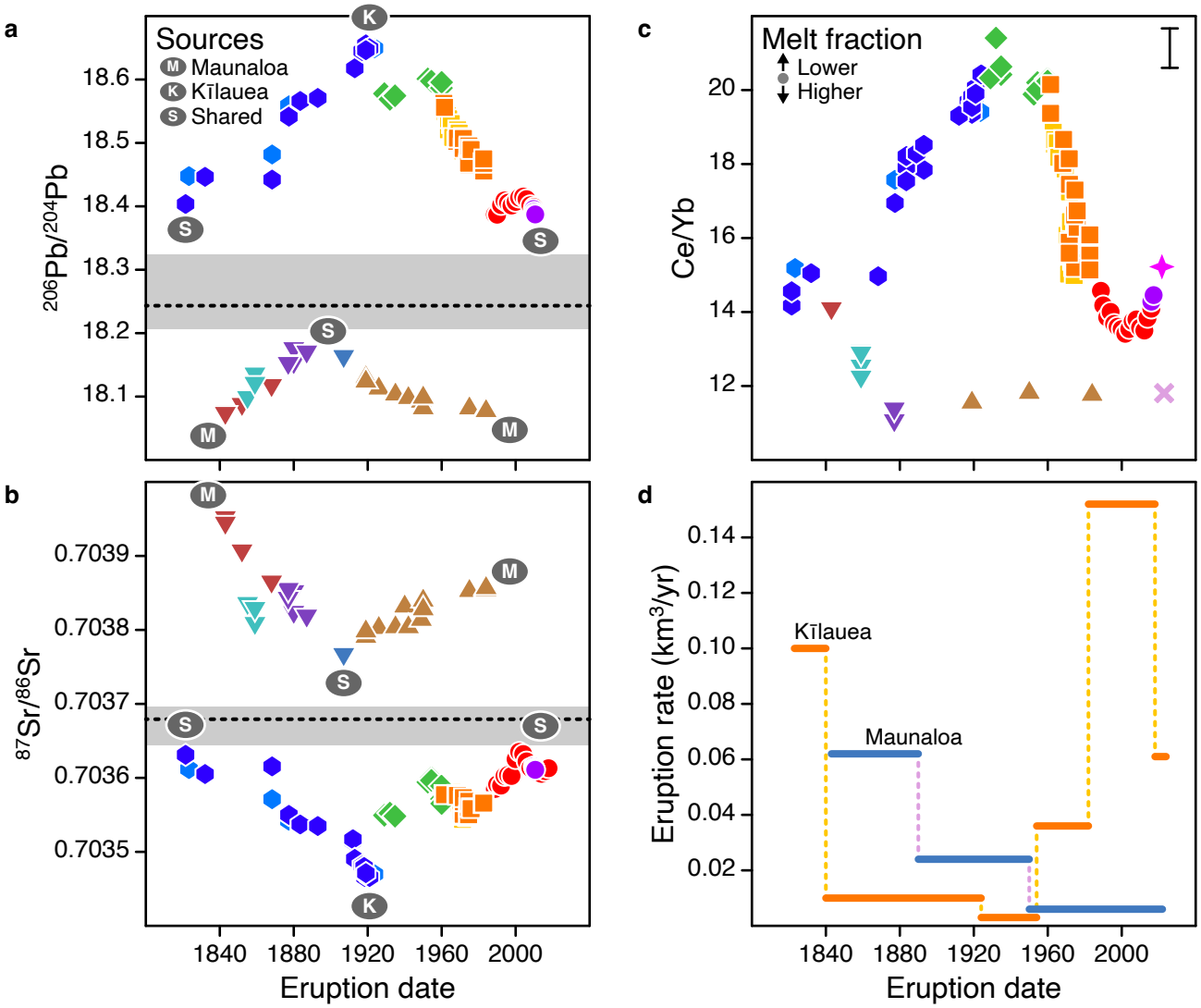
a
Sources
M Maunaloa
K Kīlauea
S Shared
$^{206}Pb/^{204}Pb$
18.6
18.5
18.4
18.3
18.2
18.1
b
$^{87}Sr/^{86}Sr$
0.7039
0.7038
0.7037
0.7036
0.7035
1840
1880
1920
1960
2000
Eruption date
c
Melt fraction
Lower
Higher
Ce/Yb
20
18
16
14
12
d
Eruption rate (km^3/yr)
0.14
0.12
0.10
0.08
0.06
0.04
0.02
Kīlauea
Maunaloa
1840
1880
1920
1960
2000
Eruption date

Figure 4

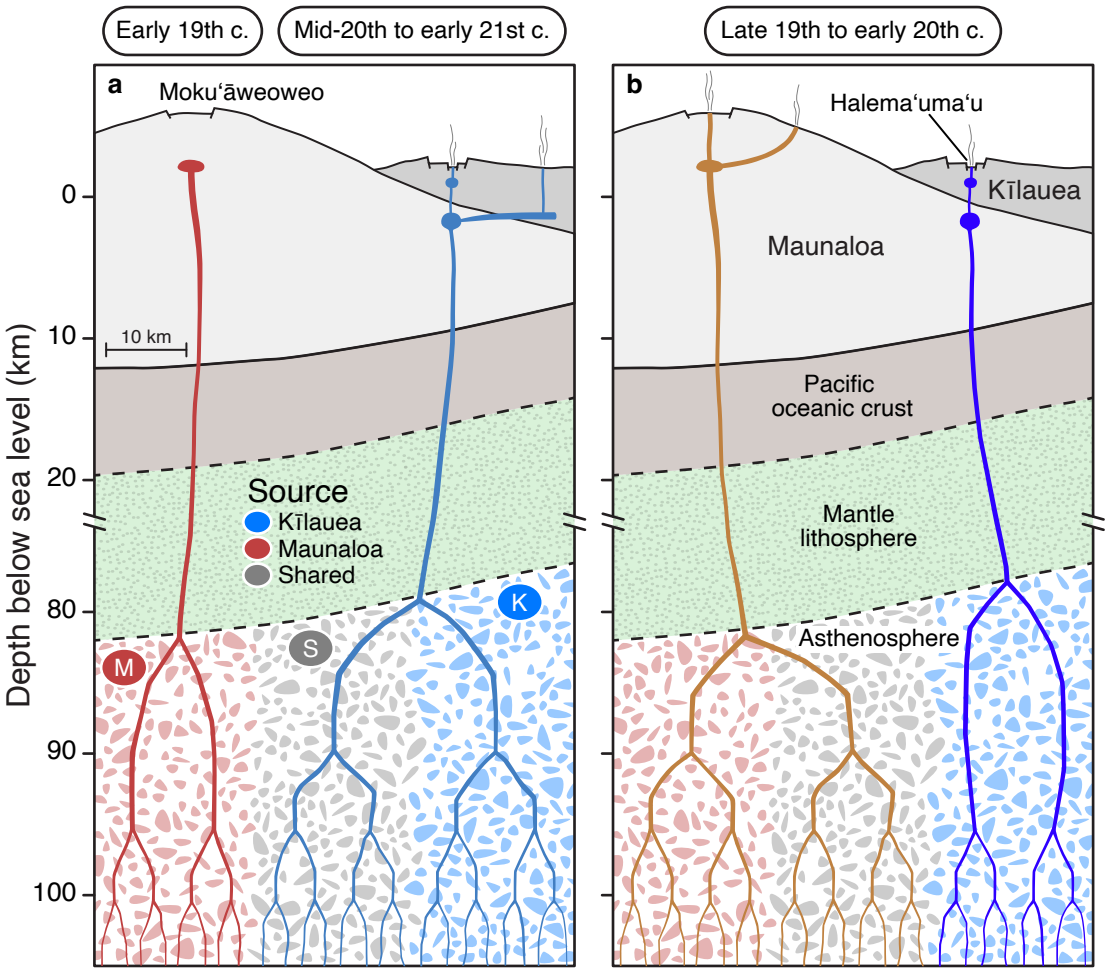
Early 19th c.
Mid-20th to early 21st c.
Late 19th to early 20th c.
a
Moku‘āweoweo
b
Halema‘uma‘u
Kīlauea
Maunaloa
Depth below sea level (km)
0
10
20
80
90
100
10 km
Source
Kīlauea
Maunaloa
Shared
Pacific
oceanic crust
Mantle
lithosphere
Asthenosphere
K
S
M

Figure S1

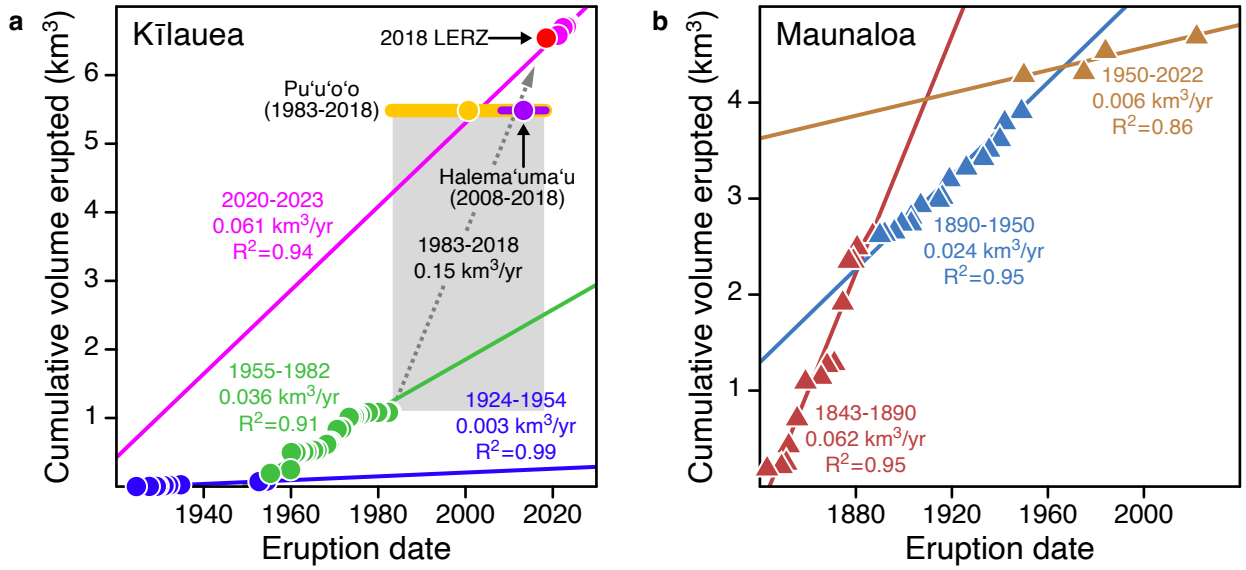
a
Kīlauea
2018 LERZ
Pu'u'o'o
(1983-2018)
Halema'uma'u
(2008-2018)
2020-2023
0.061 km3/yr
R2=0.94
1983-2018
0.15 km3/yr
1955-1982
0.036 km3/yr
R2=0.91
1924-1954
0.003 km3/yr
R2=0.99
Cumulative volume erupted (km3)
Eruption date
b
Maunaloa
1950-2022
0.006 km3/yr
R2=0.86
1890-1950
0.024 km3/yr
R2=0.95
1843-1890
0.062 km3/yr
R2=0.95
Cumulative volume erupted (km3)
Eruption date